JACS Au
AN OPEN ACCESS JOURNAL OF THE AMERICAN CHEMICAL SOCIETY

pubs.acs.org/jacsau

Article

Probing the Genuine Carrier Dynamics of Semiconducting Perovskites under Sunlight

Bo-Han Li,[▽] Huang Li,[▽] Haipeng Di,[▽] Zhipeng Xuan,[▽] Wen Zeng, Jia-Cheng Wang, Da-Bing Cheng, Chuanyao Zhou, Xingan Wang, Yiying Zhao, Jingquan Zhang,* Zefeng Ren,* and Xueming Yang

Cite This: *JACS Au* 2023, 3, 441−448

Read Online

ACCESS | Metrics & More | Article Recommendations | Supporting Information

ABSTRACT: Understanding the nature of photogenerated carriers and their subsequent dynamics in semiconducting perovskites is important for the development of solar cell materials and devices. However, most ultrafast dynamic measurements on perovskite materials were conducted under high carrier densities, which likely obscures the genuine dynamics under low carrier densities in solar illumination conditions. In this study, we presented a detailed experimental study of the carrier density-dependent dynamics in hybrid lead iodide perovskites from femtosecond to microsecond using a highly sensitive transient absorption (TA) spectrometer. From the dynamic curves with low carrier density in the linear response range, we observed two fast trapping processes that occurred in less than 1 ps and tens of picoseconds, attributed to the shallow traps, and two slow decays with lifetimes of hundreds of nanoseconds and longer than 1 μs, related to the trap-assisted recombination and trapping at deep traps. Further TA measurements clearly show that $PbCl_2$ passivation can effectively reduce both shallow and deep trap densities. These results provide insights into the intrinsic photophysics of semiconducting perovskites with direct implications for photovoltaic and optoelectronic applications under sunlight.

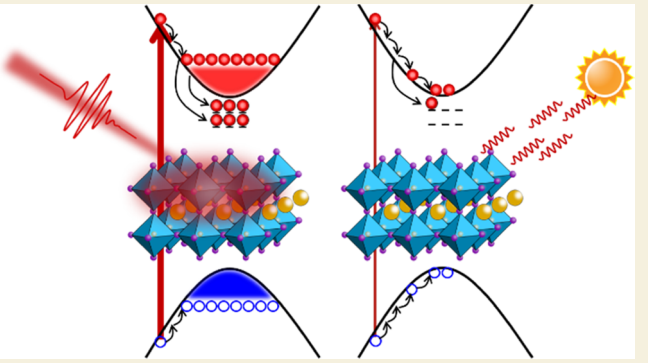

KEYWORDS: *perovskite, linear response, ultrafast carrier dynamics, low carrier density, under sunlight*

INTRODUCTION

Solar cell technology is considered one of the best energy shortage solutions for reducing carbon emissions. Over the last decade, perovskite-based solar cells have attracted significant attention and developed rapidly because of their high power conversion efficiency and low fabrication cost, making them one of the most promising solar cell materials.[1,2] The extraordinary photovoltaic performance of perovskite-based solar cells can be attributed to their strong light absorption,[3] high carrier mobility,[4,5] and long charge diffusion length.[6,7] Recent progress has been made to improve photovoltaic efficiency in fabrication protocols,[8,9] chemical compositions,[10,11] and phase stabilization methods.[12,13] Meanwhile, intense research efforts have also been made to understand these fundamental photophysical mechanisms.[14−17]

Charge- and energy-transfer processes occur in solar energy harvesting systems from femtosecond to nanosecond time scales, and understanding these processes is the key to determining the design principle for photovoltaic materials and devices.[17] Ultrafast spectroscopy, especially transient absorption (TA) spectroscopy, is employed to successfully elucidate the carrier dynamics in perovskites, such as the band filling effects,[18] hot phonon bottleneck,[19] and Auger heating.[20] However, the sensitivity of TA spectroscopy is limited; so most reported TA measurements were conducted with a high pump intensity, which induces much higher carrier densities, such as 10^{17} cm^{-3}, than that under air mass (AM) 1.5G solar illumination conditions.[16] Under steady-state AM 1.5G conditions, the calculated carrier density only reaches 4×10^{14} cm^{-3} for high-quality methylammonium lead iodide ($MAPbI_3$) films with a monomolecular lifetime of 100 ns and in the absence of charge extraction.[16] Obviously, carrier−carrier interactions at high carrier densities are bound to obscure studies of the intrinsic carrier dynamics under solar illumination.[18] Hence, to determine the genuine photogenerated carrier dynamics related to solar cells under sunlight, measurements under low carrier densities are necessary.[21]

Here, we report the photogenerated carrier dynamic research in an organometal hybrid perovskite cesium formamidinium lead iodide ($Cs_{0.1}FA_{0.9}PbI_3$) thin film in a large time scale, from hundred femtoseconds to microsecond.

Received: October 24, 2022
Revised: December 20, 2022
Accepted: December 20, 2022
Published: January 26, 2023

https://doi.org/10.1021/jacsau.2c00581
JACS Au 2023, 3, 441−448

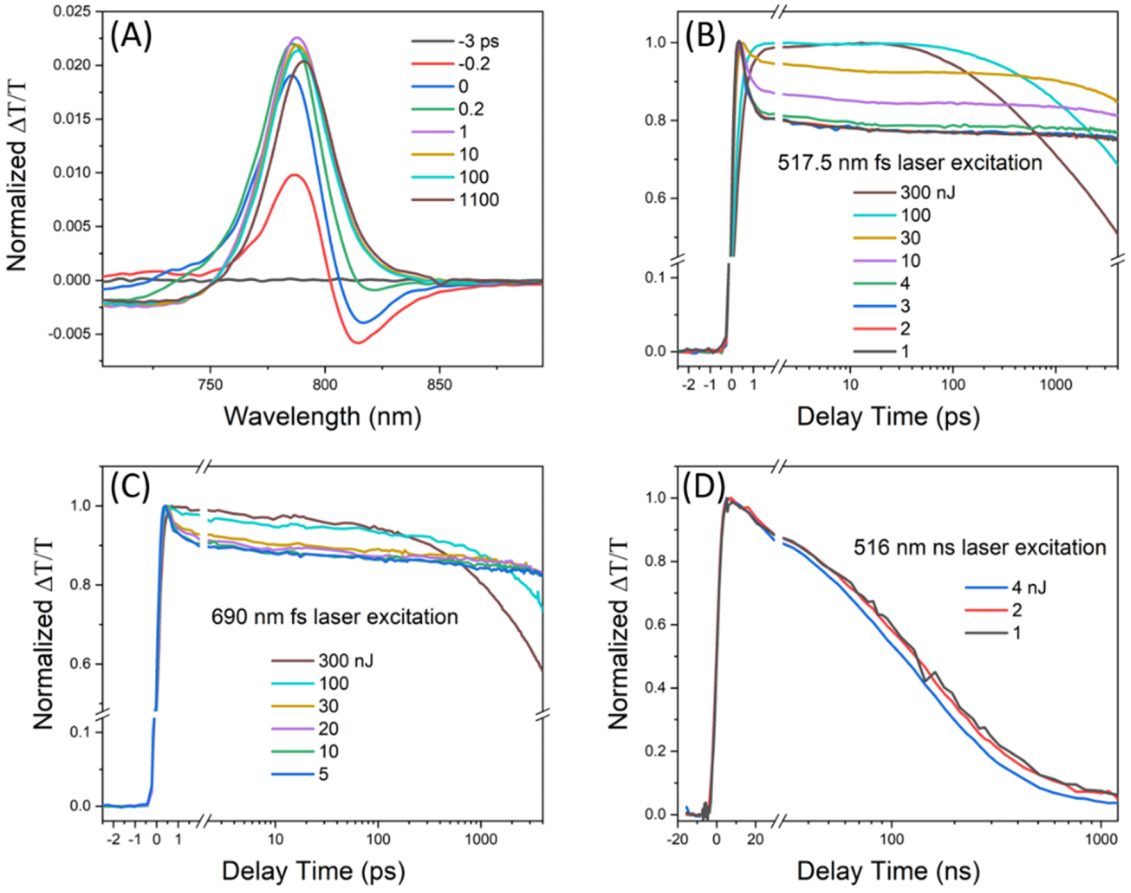

Figure 1. TA spectra and pump intensity-dependent carrier dynamics of $Cs_{0.1}FA_{0.9}PbI_3$ thin films. (A) TA spectra at different probe delay times following a 517.5 nm fs laser excitation with a pump energy of 50 nJ per pulse and a light spot diameter of 3 mm. Pump intensity-dependent TA dynamics pumped with (B) 517.5 nm and (C) 690 nm (light spot diameter about 3.5 mm) femtosecond laser pulses and (D) 516 nm (light spot about 4 × 2.5 mm^2) nanosecond laser pulse and probed at 790 nm. The normalized changes of transmission $\Delta T/T$ were plotted with different pump energies per pulse. Note the shift in time scale from linear to logarithmic, corresponding to the scale break.

It was measured by a highly sensitive TA spectrometer we recently developed, which enabled us to investigate the carrier dynamics under very low carrier densities. The TA experimental results revealed that carrier dynamics is highly carrier density-dependent. The dynamics in the linear response range showed two fast carrier decays, less than 1 ps and tens of picoseconds, attributed to trapping at shallow trap states, and two slow decay processes, hundreds of nanoseconds and about 1 μs, related to the trap-assisted recombination and trapping at deep traps. Both shallow and deep trap state densities can be effectively passivated with $PbCl_2$ in precursors. These high-sensitivity dynamic measurements reflect the genuine carrier behavior of the perovskite material under sunlight.

RESULTS AND DISCUSSION

Transient Absorption Spectra

$Cs_{0.1}FA_{0.9}PbI_3$ thin films were chosen to demonstrate the perovskite carrier dynamics under solar illumination since a partial substitution of Cs^+ for $HC(NH_2)_2^+$ (FA^+)in $FAPbI_3$ perovskite was proved to substantially improve photo- and moisture stabilities along with photovoltaic performance.[22] $Cs_{0.1}FA_{0.9}PbI_3$ thin films were prepared using a one-step method (see the Materials and Methods section). To investigate the carrier dynamics of solar energy materials under very low carrier densities, a highly sensitive TA spectrometer was developed.[23] A sensitivity level ($\Delta T/T$) of 10^{-7} was achieved by a novel technique of combining a 1 kHz macropulse and a 200 kHz high repetition micropulse and using a balanced detector scheme. Limited by the length of the delay stage, the TA dynamics from ns to μs was achieved by electronically synchronizing a diode laser and a fiber laser. More details of the TA spectrometer are described in the Materials and Methods section.

To obtain the basic TA spectral features, we conducted ensemble TA spectral measurements of the $Cs_{0.1}FA_{0.9}PbI_3$ thin film under a high pump intensity at different time delays. The TA spectra pumped at 50 nJ and 517.5 nm are shown in Figure 1A. The carrier density is estimated as 2.6 × 10^{15} cm^{-3} corresponding to 1 nJ pump light at 517.5 nm with a light spot diameter of 3 mm and 6.7 × 10^{14} cm^{-3} corresponding to 1 nJ pump light at 690 nm with a diameter of 3.5 mm (see the Supporting Information, SI). We observed that both TA dynamics were very similar. Immediately after photoexcitation, a ground-state bleaching (GSB, positive change of transmission $\Delta T/T$) band centered at about 790 nm was observed, which is consistent with the band gap obtained from the static absorption spectrum shown in Figure S3. In addition, a photoinduced absorption (PIA, negative $\Delta T/T$) band centered at around 815 nm was observed. The GSB feature is mainly attributed to the band filling, which is the presence of photogenerated band-gap carriers blocking the optical absorption of the probe pulse. The PIA was possibly from

https://doi.org/10.1021/jacsau.2c00581
JACS Au 2023, 3, 441−448

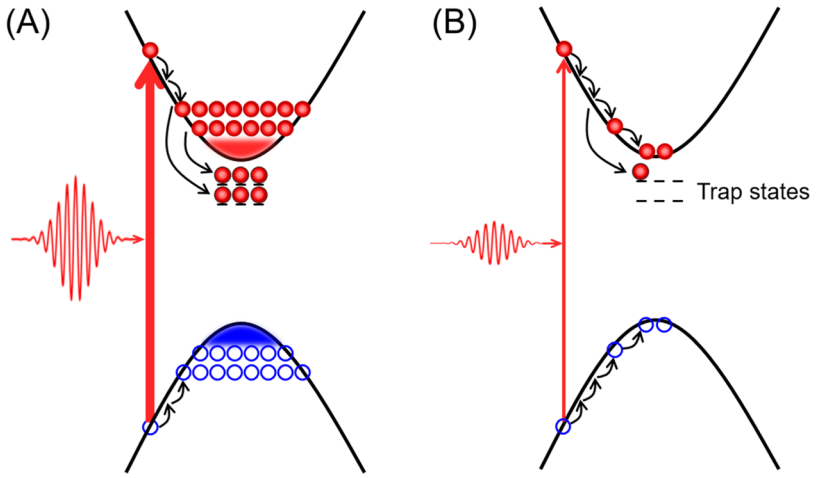

Figure 2. Schematic model of pump intensity-dependent carrier dynamics. (A) High carrier density generated by high-intensity pumping. High carrier density-induced hot phonon bottleneck effect and band-gap renormalization. A small percentage of carriers are trapped due to the limited trap state density. (B) Low carrier density generated by low-intensity pumping. A certain percentage of carriers are trapped, proportional to the trap state density. Hole trapping is not indicated in the schematic.

the excited-state absorption of the hot carriers or due to the band-gap shift induced by hot carriers.[24] After 1 ps, the PIA disappeared. The GSB lifetime was longer than 1 ns.

Carrier Density-Dependent Carrier Dynamics

To elucidate the carrier recombination mechanism over a range of excitation intensities, the dynamic curve can be modeled by the simple rate equation

$$-\frac{dn}{dt} = An + Bn^2 + Cn^3 \quad (1)$$

where n is the photogenerated carrier density and t is the time. The values of the rate coefficients A, B, and C for each term successively reduce by multiple orders of magnitude.[16] Each term in eq 1 is ascribed to different physical carrier annihilation processes: (1) monomolecular Shockley−Read−Hall recombination, also called trap-assisted recombination, and geminate recombination, which is relatively insignificant for three-dimensional (3D) perovskites at room temperature,[25] (2) bimolecular free carrier direct recombination, and (3) three-body Auger recombination. The carrier dynamics is highly dependent on the carrier density. The bimolecular and Auger recombination mechanisms were mostly used to elucidate the carrier density decay processes in the reported TA studies, owing to high carrier densities. Figure 1B shows the normalized dynamic traces of the GSB signals at 790 nm for various pump intensities by more than 2 orders of magnitude with a 517.5 nm femtosecond laser excitation. Some obvious features can be clearly resolved. First, the rising edge of the GSB signal, which corresponds to the carrier excitation and cooling processes, is slower at high pump intensities. This is caused by the hot phonon bottleneck effect, which reduces the hot carrier cooling rate when a high density of carriers is excited[16,19] (see Figure 2A). Second, an ultrafast decay process within 1 ps appears at low pump intensities, and another fast decay process is in the tens of picosecond scale. These two processes are attributed to the trapping processes by shallow trap states, whose assignments will be discussed below. In addition, the fast decay process is absent under high carrier densities since the percentage of free carriers by trapping is too small because of the limited carrier trap density, as shown in Figure 2A. While a considerable percentage of free carriers can be trapped under low carrier densities, illustrated in Figure 2B, and can be sufficiently resolved in TA measurements. Third, at a delay range of 100−3500 ps, the decay rate of the GSB signal slows down with decreasing pump intensity. This is caused by the low bimolecular and Auger decay rates and the dominated monomolecular process at low carrier densities.[16,18,26] Fourth, when the pump energy is below 3 nJ, the normalized TA curves reach the linear response range, independent of the pump intensity. That is, only the monomolecular process occurs dominantly, without any nonlinear process, under very low carrier density.

Several factors can affect carrier dynamics. Reports have shown that the band-gap renormalization energy in $FAPbI_3$ under a carrier density of 3.8×10^{16} cm^{-3} was 0.44 meV.[19] In this study, the carrier density is less than 10^{16} cm^{-3} in the linear response range, so the band-gap renormalization can be neglected. The formation of excitons can reduce the free carrier density. Due to the small binding energy of excitons, they can also be excluded at room temperature.[25] In addition, considering the equilibrium between the formation and ionization of excitons, as described by the reaction

$$e + h \leftrightarrows \text{exciton}$$

when the photogenerated carrier density decreases, the equilibrium shifts toward the formation of free carriers. Thus, the GSB signal decay at 790 nm is only caused by a decline in the free carrier density. Recombination has often been considered the main cause of inducing carrier density decay. Both the bimolecular and Auger recombination processes could be excluded as they exhibited strong carrier density dependence and only dominated in high carrier densities.[16] In this study, the pump intensity was sufficiently low that the carrier dynamics reached the linear response range. Hence, only trapping and trap-assisted recombination are possible. However, trap-assisted recombination usually lasts tens or even hundreds of nanoseconds.[16] Further, these two fast decay processes reach equilibrium very quickly. If they are from the trapping at deep traps, that is, without the detrapping process, the decay will continue without reaching equilibrium. While photogenerated free carriers are trapped by the shallow traps, as the density of trapped carriers increases and the

https://doi.org/10.1021/jacsau.2c00581
JACS Au 2023, 3, 441−448

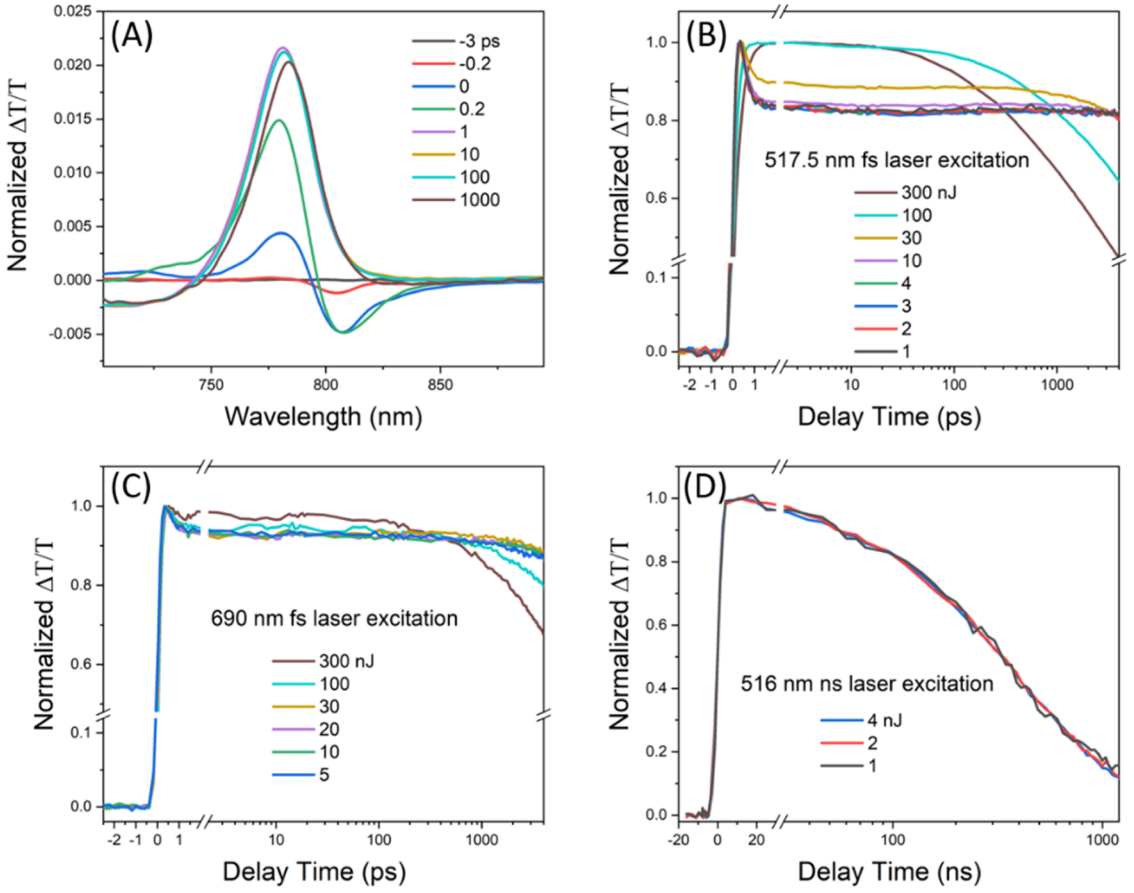

Figure 3. $PbCl_2$ passivation effect. (A) TA spectra of $PbCl_2$ passivated thin films at different probe delay times following a 517.5 nm femtosecond laser excitation with a pump energy of 50 nJ per pulse and a light spot diameter of about 3 mm. Pump intensity-dependent TA dynamics pumped with (B) 517.5 nm and (C) 690 nm (light spot diameter about 3.5 mm) femtosecond laser pulses and (D) 516 nm (light spot about 4×2.5 mm^2) nanosecond laser pulse and probed at 780 nm. The normalized changes of transmission $\Delta T/T$ were plotted with different pump energies per pulse.

density of free carriers decreases, the trapping rate slows down while the detrapping rate increases. Finally, the trapping and detrapping processes reach the equilibration. The detailed model of carrier dynamics with shallow traps is described in the Supporting Information. Therefore, we attribute these fast decays to carriers trapping by shallow trap states. This has also been widely observed in oxides,[27] perovskite nanocrystals,[14,28] carbon films,[29] and two-dimensional (2D) materials.[30] And the long decay process is ascribed to trap-assisted recombination or trapping by deep traps.

To further investigate the carrier dynamics with different pump wavelengths, the TA spectra under a 690 nm femtosecond laser excitation at different time delays were measured (Figure S7). The pump intensity-dependent TA dynamics with a probe wavelength at 790 nm is shown in Figure 1C, and the main features of the dynamic curves are very similar to Figure 1B. Compared to the dynamics pumped at 517.5 nm, one difference is that the pump energy of 10 nJ reaches the linear response range, which is consistent with the carrier density due to the low absorption coefficient at 690 nm. The second is that the amplitude of the ultrafast decay process within 1 ps is obviously smaller, and another obvious feature is that the long decay process is faster, both of which will be discussed in detail below.

We can find that the carrier lifetime is very long under low carrier density, and we cannot deduce the full dynamics by the limited range of the optical delay stage. Here, the newly developed nanosecond resolution TA spectrometer was employed, which can share the same sample, probe light, and data collection system. Figure 1D shows the pump intensity-dependent dynamic curves with a 516 nm nanosecond laser excitation, which indicates a similar trend as femtosecond resolution TA curves. A pump energy of about 2 nJ enters into the linear response range. The carrier lifetime shows up to more than 100 ns. The carrier densities generated by the 3 nJ pump light at 517.5 nm and 10 nJ at 690 nm are 7.8 $\times 10^{15}$ and 6.7 $\times 10^{15}$ cm^{-3}, respectively, which indicates the upper limit of carrier density in the linear response range. This is the first time to obtain the intrinsic carrier dynamics of three-dimensional perovskites under solar illumination using TA spectroscopy.

Passivation Effects with $PbCl_2$

Trap-assisted recombination is considered one of the most detrimental factors to solar cell performance.[2,25,31] In solar cell materials, deep trap states can effectively induce high trap-assisted recombination rates and low carrier mobility, causing the reduction of open-circuit voltage and loss of short-circuit current. These issues can also be partially caused by shallow trap states, although shallow trap states are not efficient recombination centers and the carriers can be detrapped by thermal excitations. In addition, trap states also accelerate the degradation of the perovskite solar cell.[32,33] Therefore, it has promoted numerous passivation techniques to reduce the trap state density in perovskite solar cells.[34−37] Here, we have

https://doi.org/10.1021/jacsau.2c00581
JACS Au 2023, 3, 441−448

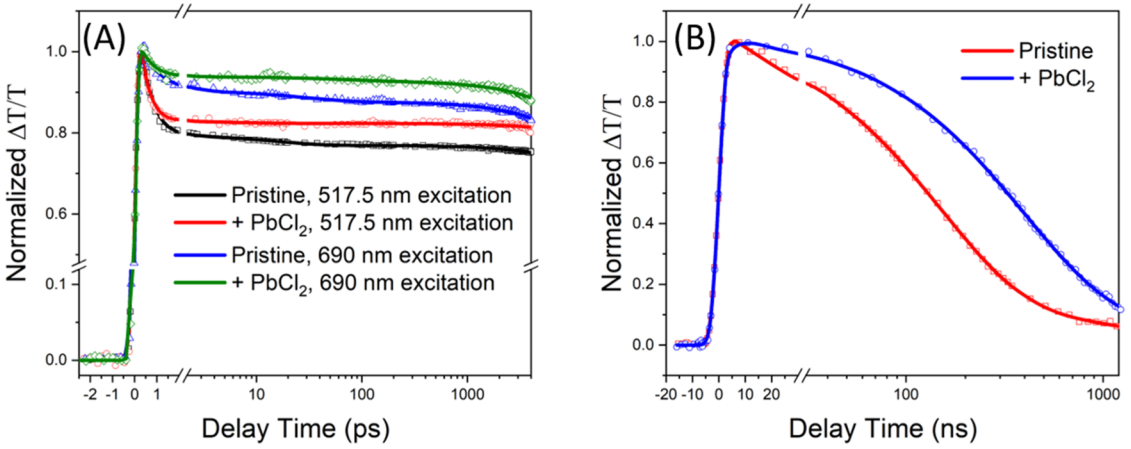

Figure 4. Comparison of passivation effects in the linear response range. (A) Carrier dynamics of pristine and $PbCl_2$-passivated thin films excited by (A) 517.5 and 690 nm femtosecond laser and (B) 516 nm nanosecond laser. Dots are original data, and lines are fitting results.

investigated the passivation effects by adding $PbCl_2$ in the precursor solution to form mixed lead iodide perovskites by TA dynamics. Figure 3A shows that the GSB peak of the $PbCl_2$-passivated perovskites is about 780 nm, a small blue shift from the GSB peak of the pristine perovskites at 790 nm. Similarly to the pristine sample, the TA spectra and the pump intensity-dependent carrier dynamics of the passivated sample were measured with 517.5 and 690 nm femtosecond lasers and 516 nm nanosecond laser excitations, as shown in Figure 3. The main features are the same as the pristine sample, but there are still some obvious differences in the dynamic curves. The first difference is that the pump intensity in the linear response range is higher for the passivated sample, as shown in Figure 3B–D. The second one is that the amplitude of the ultrafast decay within 1 ps is reduced, and the decay in the tens of picosecond scale seems gone. Furthermore, the carrier lifetime is unambiguously much longer than the pristine sample under low carrier density. These results indicate that the passivation of $PbCl_2$ can effectively reduce the deep trap density and reduce the shallow level defect to some extent. It was reported that the presence of chloride ions during growth results in larger crystal sizes.[38,39] Since larger crystallites mean smaller interfacial area, trap states, especially deep trap states mainly located at the crystallite surface/interface,[40] can be largely reduced. The larger crystals grown with chloride ions also feature well-defined facets of low Miller indices[38] and coherent long-range packing of the crystals in the film.[39] Negligible trapping on low-index crystalline faces of the perovskite crystal was proposed by theoretical calculations.[41] Moreover, the trap states can also be effectively healed by close interaction between the well-defined facets of neighboring crystals in a coherently packed film.[14]

Quantitative Analysis of Carrier Dynamics in the Linear Response Range

Due to the importance of traps in perovskite solar cells, many techniques have been developed to probe trap states.[42−45] Recently, the spatial and energetic distributions of trap states in metal halide perovskite single-crystalline and polycrystalline solar cells were quantitatively measured using the drive-level capacitance profiling (DLCP) method.[40] The researchers found that most of the deep traps were located at the crystal surfaces and interfaces of the polycrystalline films, even after surface passivation. However, these static and kinetic measurements are not enough to comprehensively understand the impact of charge traps on charge transport in perovskite materials and devices on a microscopic level. The trapping process can also be directly observed by probing the bleaching of trapped carrier below the optical gap,[14] but it is still difficult to obtain the beaching signal of all of the trapping carriers owing to the wide energetic distributions of the trap states and the normally low trap state density per unit energy.[40] In this work, the fast GSB depletion of free carriers is a direct reflection of the quantity of trapped carriers at shallow traps, and the long lifetime dynamics of carriers reflects the trap-assisted recombination and trapping by deep traps. Note that this is different from the trap states measured by DLCP. This reported trap state mainly consisted of deep trap states greater than 0.24 eV, which is about 10 times the thermal energy at room temperature.[40] Different trap states have different carrier capture cross sections, related to the type of trapped carriers, the energy depth, spatial distribution, which are subject to sample processing and handling conditions, and temperature.[16,46] The GSB probed in TA in this work includes all effects from the traps with broader energetic ranges, as long as they reduce the free carrier density, through either trapping carriers or acting as recombination centers.

To quantitatively obtain the genuine carrier dynamics and understand the influence of traps on dynamics, we analyzed the dynamic curves in the linear response range. Figure 4 replots the dynamic curves of pristine and $PbCl_2$-passivated thin films under the low carrier density condition and shows the fitting curves as well based on eq S4, using a function of triple exponential decay convoluted with a time resolution function. Table S1 summarizes the fitting results.

For the pristine thin film, a fast decay process shows as short as less than 500 fs with an excitation of 517.5 nm light, while a little longer for a low photon energy excitation of 690 nm. In addition, the proportion of the fast decay for the pump wavelength at 690 nm is much smaller than at 517.5 nm. It is because the pump light at 517.5 nm has a much larger absorption coefficient than at 690 nm, which induces the carriers created by the 517.5 nm pump that are spatially distributed more concentrated near the surface. So, the difference between the fast decay with the pump wavelengths of 517.5 and 690 nm is mainly due to the different carrier densities near the surface. It was reported that the perovskite defects are mainly concentrated on the surface,[40] carriers near the surface are more easily captured by the trap states. The fast

https://doi.org/10.1021/jacsau.2c00581
JACS Au 2023, 3, 441−448

decay rate is obviously faster at a 517.5 nm excitation than at 690 nm, which is possibly partially due to higher excess energies inducing faster carrier trapping rates, resulting from the interactions with shallow traps.[28] For the passivated thin film, the proportion of the fast decay is noticeably reduced with both excitation wavelengths. In addition, the decay rate also shows faster due to the possible change of the energy distribution of trap states and higher excess energy due to the smaller band gap.

Another fast decay lifetime is about 15 and 30 ps for excitations at 517.5 and 690 nm, respectively, for the pristine thin film. After passivation, it almost disappears. Moreover, we can also find that the longest carrier lifetime is more than 300 ns for the passivated thin film, much longer than the pristine, about 150 ns. These imply that both the density of trap states and recombination centers are dramatically reduced by $PbCl_2$ passivation. However, the carrier lifetime with a 690 nm excitation shows shorter than that with a 517.5 nm excitation. This can be clearly explained from eq S16. Larger trapping at shallow traps, corresponding to larger k_1/k_2, can lead to slow trap-assisted recombination slower; that is, trapping at shallow traps prolongs the carrier lifetime. In this regard, an appropriate density of shallow traps is beneficial to the solar cell. Fitting results in Figure 4B also show another very slow decay process, longer than 1 μs, which can be attributed to the slow recombination process from deep trap states. Its model is described in detail in the SI.

According to reports on $MAPbI_3$ solar cells,[7] electron transfer to the electron transport layer occurs within 400 ps, while holes transferred to the hole transport layer occur within 650 ps. Here, the carrier lifetime was determined as several hundreds of nanoseconds, much longer than the charge transport time. Hence, it seems that the deep trap has little effect on the charge transfer. However, this is contradictory to a common understanding. It is worth noting that these charge transport times were obtained by TA measurements at high carrier density conditions, so further work on determining the charge transport time is necessary at low carrier density conditions in the future.

CONCLUSIONS

We obtained ultrafast carrier dynamics of $Cs_{0.1}FA_{0.9}PbI_3$ perovskite thin films under different carrier densities. At a very low carrier density in the linear response range, the genuine carrier dynamics under sunlight illumination was determined. Based on it, we have observed that two fast trapping processes occurred in less than 1 ps and tens of picoseconds, attributed to the shallow traps, and two slow decays with lifetimes of hundreds of nanoseconds and longer than 1 μs, related to the trap-assisted recombination and trapping at deep traps. Both kinds of trap densities can be effectively reduced by $PbCl_2$ passivation. These results not only provide a fundamental understanding of the intrinsic photophysical behavior of perovskites under solar illumination conditions but also provide a better method for assessing the performance of perovskite solar cell materials.

MATERIALS AND METHODS

Preparation and Characterization of Perovskite Films

Perovskite films were prepared using the one-step method. The Corning glass substrates with a dimension of 1.5 × 1.5 cm^2 were soaked in detergent for 2 h, followed by ultrasonic cleaning for 15 min in absolute ethanol, deionized water, and absolute ethanol sequentially, and then blow-dried with N_2 gas for later use. The substrates were further treated with ultraviolet−ozone for 15 min before use. The precursor solution was prepared by dissolving 0.9 mmol of formamidinium iodide (FAI, >99.99%, Greatcell), 0.1 mmol of CsI (>99.9%, Xi'an PLT), and 1 mmol of PbI_2 (>99.99%, TCI) into 1 mL of *N*,*N*-dimethylformamide (DMF, anhydrous, >99.8%, Sigma-Aldrich)/dimethyl sulfoxide (DMSO, anhydrous, >99.9%, Sigma-Aldrich) (9:1 volume ratio) and stirring sufficiently. The perovskite precursor solution was spin-coated at 1000 rmp for 10 s and at 6000 rpm for 15 s on the prepared substrate. The antisolvent of chlorobenzene (CB, anhydrous, >99.5%, Sigma-Aldrich) was injected on the spinning substrate constantly for about 10 s finally. All of the samples were then annealed at 100 °C for 10 min on a hot stage. The 5% $PbCl_2$ (>99.9%, Xi'an PLT) passivated sample was prepared in the same way. All of the preparation was conducted inside a nitrogen-filled glovebox. X-ray diffraction spectra were recorded by an X-ray diffractometer (LabX XRD-6100 SHIMADZU). The ultraviolet−visible (UV−vis) absorption spectra were performed by a Lambda 950 UV−vis spectrophotometer (PerkinElmer Inc.). The surface morphology was measured by the Zeiss field emission SEM (Hitachi S-4800) equipped with EDS.

Transient Absorption Measurements

The transient absorption measurements were based on a fiber laser (1030 nm, pulse duration of ∼230 fs, 1 MHz repetition rate) and a recently developed pump−probe transient absorption spectrometer.[23] A sensitivity level ($\Delta T/T$) of 10^{-7} was achieved by a novel technique of combining macropulse and micropulse and using a balanced detector scheme. The repetition rate of the fundamental beam output was divided down to 200 kHz from 1 MHz as micropulses and then modulated at 1 kHz as macropulse. The number of micropulses in a macropulse can be selected based on the signal-to-noise ratio. The output was split into two beams. One beam was to generate second harmonics (517.5 nm) or sent to an optical parametric amplifier (CHOPAS-G, BC-Light) to generate the pump pulse, and its intensity was tuned by the combination of a half waveplate and a polarization beamsplitter (PBS). The pump light was modulated at 500 Hz of macropulses by a chopper. The other beam of 1030 nm was focused into a sapphire crystal to generate supercontinuum. Then, it was split into two beams by using an achromatic waveplate and a PBS. One enters a monochromator and was collected by a photodiode (PD) as the reference light, and the other was focused and then passed through the sample as the probe light, collimated and dispersed with a monochromator, and finally probed by the other PD, with an integrating 3 nm bandwidth (FWHM) of the probe light. Both PDs were connected to a balanced transimpedance amplifier and then a lock-in amplifier. The pump−probe delay can be up to ∼4 ns tuned by a delay line. The pump and probe were focused and overlapped onto the sample. The pump size is about diameter (d) 3 mm for 517.5 nm and about diameter (d) 3.5 mm for 690 nm, and the probe size is about diameter (d) 0.6 mm. For the TA measurements in a longer time delay, a diode laser (516 nm, FWHM 2.2 nm, NPL52C, Thorlabs) was used as the pump, which was synchronized with the fiber laser. Their delay was electronically tuned with a delay generator.

ASSOCIATED CONTENT

Supporting Information

The Supporting Information is available free of charge at https://pubs.acs.org/doi/10.1021/jacsau.2c00581.

Sample characterization; test of sample stability; initial carrier density estimation; pump intensity-dependent TA dynamics at a pump wavelength of 690 nm; fitting results; and photogenerated carrier dynamics models with shallow and deep traps (PDF)

https://doi.org/10.1021/jacsau.2c00581
JACS Au 2023, 3, 441−448

AUTHOR INFORMATION

Corresponding Authors

Jingquan Zhang − *Institute of Solar Energy Materials and Devices, College of Materials Science and Engineering, Sichuan University, Chengdu 610065, China;* orcid.org/0000-0002-5346-2730; Email: zhangjq@scu.edu.cn

Zefeng Ren − *State Key Laboratory of Molecular Reaction Dynamics and Dynamics Research Center for Energy and Environmental Materials, Dalian Institute of Chemical Physics, Chinese Academy of Sciences, Dalian 116023, China;* orcid.org/0000-0002-5263-9346; Email: zfren@dicp.ac.cn

Authors

Bo-Han Li − *State Key Laboratory of Molecular Reaction Dynamics and Dynamics Research Center for Energy and Environmental Materials, Dalian Institute of Chemical Physics, Chinese Academy of Sciences, Dalian 116023, China; University of Chinese Academy of Sciences, Beijing 100049, China*

Huang Li − *State Key Laboratory of Molecular Reaction Dynamics and Dynamics Research Center for Energy and Environmental Materials, Dalian Institute of Chemical Physics, Chinese Academy of Sciences, Dalian 116023, China; Department of Chemical Physics, University of Science and Technology of China, Hefei 230026, China*

Haipeng Di − *Institute of Materials, China Academy of Engineering Physics, Jiangyou 621908, China*

Zhipeng Xuan − *Institute of Solar Energy Materials and Devices, College of Materials Science and Engineering, Sichuan University, Chengdu 610065, China*

Wen Zeng − *State Key Laboratory of Molecular Reaction Dynamics and Dynamics Research Center for Energy and Environmental Materials, Dalian Institute of Chemical Physics, Chinese Academy of Sciences, Dalian 116023, China; University of Chinese Academy of Sciences, Beijing 100049, China*

Jia-Cheng Wang − *State Key Laboratory of Molecular Reaction Dynamics and Dynamics Research Center for Energy and Environmental Materials, Dalian Institute of Chemical Physics, Chinese Academy of Sciences, Dalian 116023, China; University of Chinese Academy of Sciences, Beijing 100049, China*

Da-Bing Cheng − *State Key Laboratory of Molecular Reaction Dynamics and Dynamics Research Center for Energy and Environmental Materials, Dalian Institute of Chemical Physics, Chinese Academy of Sciences, Dalian 116023, China*

Chuanyao Zhou − *State Key Laboratory of Molecular Reaction Dynamics and Dynamics Research Center for Energy and Environmental Materials, Dalian Institute of Chemical Physics, Chinese Academy of Sciences, Dalian 116023, China;* orcid.org/0000-0002-3252-2992

Xingan Wang − *Department of Chemical Physics, University of Science and Technology of China, Hefei 230026, China;* orcid.org/0000-0002-1206-7021

Yiying Zhao − *Institute of Materials, China Academy of Engineering Physics, Jiangyou 621908, China;* orcid.org/0000-0002-1424-2516

Xueming Yang − *State Key Laboratory of Molecular Reaction Dynamics and Dynamics Research Center for Energy and Environmental Materials, Dalian Institute of Chemical Physics, Chinese Academy of Sciences, Dalian 116023, China; Department of Chemistry, Southern University of Science and Technology, Shenzhen 518055, China;* orcid.org/0000-0001-6684-9187

Complete contact information is available at: https://pubs.acs.org/10.1021/jacsau.2c00581

Author Contributions

[▽]B.L., H.L., H.D., and Z.X. contributed equally to this work. B.L., X.Y., and Z.R. conceived and designed experiments. B.L., H.L., H.D., W.Z., J.W., D.C., and Z.R. set up the transient absorption spectrometer and carried out the transient absorption measurements. H.D., Z.X., Y.Z., and J.Z. prepared the perovskite samples. Z.X. and J.Z. performed characterizations. B.L., H.L., C.Z., J.Z., and Z.R. analyzed the data. B.L., J.Z., X.Y., and Z.R. wrote the manuscript with inputs from all authors.

Notes

The authors declare no competing financial interest.

ACKNOWLEDGMENTS

This work was supported by the Ministry of Science and Technology of China (2018YFA0208700, 2019YFE0120000); the Dalian Institute of Chemical Physics, Chinese Academy of Sciences (I202003); the National Natural Science Foundation of China (22073097, 21688102); the Chinese Academy of Sciences (YSBR-007); and the Science and Technology Program of Sichuan Province (2021YFG0102, 2019YFG0513, and 2019ZDZX0015).

REFERENCES

(1) Kojima, A.; Teshima, K.; Shirai, Y.; Miyasaka, T. Organometal halide perovskites as visible-light sensitizers for photovoltaic cells. *J. Am. Chem. Soc.* **2009**, *131*, 6050−6051.

(2) Kim, J. Y.; Lee, J.-W.; Jung, H. S.; Shin, H.; Park, N.-G. High-efficiency perovskite solar cells. *Chem. Rev.* **2020**, *120*, 7867−7918.

(3) Park, N.-G. Perovskite solar cells: an emerging photovoltaic technology. *Mater. Today* **2015**, *18*, 65−72.

(4) Herz, L. M. Charge-carrier mobilities in metal halide perovskites: Fundamental mechanisms and limits. *ACS Energy Lett.* **2017**, *2*, 1539−1548.

(5) Wehrenfennig, C.; Eperon, G. E.; Johnston, M. B.; Snaith, H. J.; Herz, L. M. High Charge Carrier Mobilities and Lifetimes in Organolead Trihalide Perovskites. *Adv. Mater.* **2014**, *26*, 1584−1589.

(6) Stranks, S. D.; Eperon, G. E.; Grancini, G.; Menelaou, C.; Alcocer, M. J. P.; Leijtens, T.; Herz, L. M.; Petrozza, A.; Snaith, H. J. Electron-hole diffusion lengths exceeding 1 micrometer in an organometal trihalide perovskite absorber. *Science* **2013**, *342*, 341−344.

(7) Xing, G.; Mathews, N.; Sun, S.; Lim, S. S.; Lam, Y. M.; Gratzel, M.; Mhaisalkar, S.; Sum, T. C. Long-range balanced electron- and hole-transport lengths in organic-inorganic $CH_3NH_3PbI_3$. *Science* **2013**, *342*, 344−347.

(8) Burschka, J.; Pellet, N.; Moon, S.-J.; Humphry-Baker, R.; Gao, P.; Nazeeruddin, M. K.; Grätzel, M. Sequential deposition as a route to high-performance perovskite-sensitized solar cells. *Nature* **2013**, *499*, 316−319.

(9) Yang Woon, W. S.; Park, B.-W.; Jung, E. H.; Jeon, N. J.; Kim, Y. C.; Lee, D. U.; Shin, S. S.; Seo, J.; Kim, E. K.; Noh, J. H.; Seok, S. I. Iodide management in formamidinium-lead-halide−based perovskite layers for efficient solar cells. *Science* **2017**, *356*, 1376−1379.

(10) Jeon, N. J.; Noh, J. H.; Yang, W. S.; Kim, Y. C.; Ryu, S.; Seo, J.; Seok, S. I. Compositional engineering of perovskite materials for high-performance solar cells. *Nature* **2015**, *517*, 476−480.

(11) Abdi-Jalebi, M.; Andaji-Garmaroudi, Z.; Cacovich, S.; Stavrakas, C.; Philippe, B.; Richter, J. M.; Alsari, M.; Booker, E. P.;

Hutter, E. M.; Pearson, A. J.; Lilliu, S.; Savenije, T. J.; Rensmo, H.; Divitini, G.; Ducati, C.; Friend, R. H.; Stranks, S. D. Maximizing and stabilizing luminescence from halide perovskites with potassium passivation. *Nature* **2018**, *555*, 497−501.
(12) Saliba, M.; Matsui, T.; Domanski, K.; Seo, J.-Y.; Ummadisingu, A.; Zakeeruddin Shaik, M.; Correa-Baena, J.-P.; Tress Wolfgang, R.; Abate, A.; Hagfeldt, A.; Grätzel, M. Incorporation of rubidium cations into perovskite solar cells improves photovoltaic performance. *Science* **2016**, *354*, 206−209.
(13) Min, H.; Kim, M.; Lee, S. U.; Kim, H.; Kim, G.; Choi, K.; Lee, J. H.; Seok, S. I. Efficient, stable solar cells by using inherent bandgap of α-phase formamidinium lead iodide. *Science* **2019**, *366*, 749−753.
(14) Wu, X.; Trinh, M. T.; Niesner, D.; Zhu, H.; Norman, Z.; Owen, J. S.; Yaffe, O.; Kudisch, B. J.; Zhu, X. Y. Trap states in lead iodide perovskites. *J. Am. Chem. Soc.* **2015**, *137*, 2089−2096.
(15) Zhu, H.; Miyata, K.; Fu, Y.; Wang, J.; Joshi, P. P.; Niesner, D.; Williams, K. W.; Jin, S.; Zhu, X.-Y. Screening in crystalline liquids protects energetic carriers in hybrid perovskites. *Science* **2016**, *353*, 1409−1413.
(16) Johnston, M. B.; Herz, L. M. Hybrid perovskites for photovoltaics: Charge-carrier recombination, diffusion, and radiative efficiencies. *Acc. Chem. Res.* **2016**, *49*, 146−154.
(17) Shi, J.; Li, Y.; Li, Y.; Li, D.; Luo, Y.; Wu, H.; Meng, Q. From ultrafast to ultraslow: Charge-carrier dynamics of perovskite solar cells. *Joule* **2018**, *2*, 879−901.
(18) Manser, J. S.; Kamat, P. V. Band filling with free charge carriers in organometal halide perovskites. *Nat. Photonics* **2014**, *8*, 737−743.
(19) Yang, Y.; Ostrowski, D. P.; France, R. M.; Zhu, K.; van de Lagemaat, J.; Luther, J. M.; Beard, M. C. Observation of a hot-phonon bottleneck in lead-iodide perovskites. *Nat. Photonics* **2016**, *10*, 53−59.
(20) Fu, M.; Tamarat, P.; Trebbia, J.-B.; Bodnarchuk, M. I.; Kovalenko, M. V.; Even, J.; Lounis, B. Unraveling exciton-phonon coupling in individual $FAPbI_3$ nanocrystals emitting near-infrared single photons. *Nat. Commun.* **2018**, *9*, No. 3318.
(21) Dai, L.; Deng, Z.; Auras, F.; Goodwin, H.; Zhang, Z.; Walmsley, J. C.; Bristowe, P. D.; Deschler, F.; Greenham, N. C. Slow carrier relaxation in tin-based perovskite nanocrystals. *Nat. Photonics* **2021**, *15*, 696−702.
(22) Lee, J.-W.; Kim, D.-H.; Kim, H.-S.; Seo, S.-W.; Cho, S. M.; Park, N.-G. Formamidinium and Cesium Hybridization for Photo- and Moisture-Stable Perovskite Solar Cell. *Adv. Energy Mater.* **2015**, *5*, No. 1501310.
(23) Li, H.; Hu, G.; Li, B.-H.; Zeng, W.; Zhang, J.; Wang, X.; Zhou, C.; Ren, Z.; Yang, X. Ultrahigh sensitive transient absorption spectrometer. *Rev. Sci. Instrum.* **2021**, *92*, No. 053002.
(24) Trinh, M. T.; Wu, X.; Niesner, D.; Zhu, X.-Y. Many-body interactions in photo-excited lead iodide perovskite. *J. Mater. Chem. A* **2015**, *3*, 9285−9290.
(25) Herz, L. M. Charge-carrier dynamics in organic-inorganic metal halide perovskites. *Annu. Rev. Phys. Chem.* **2016**, *67*, 65−89.
(26) Yamada, Y.; Nakamura, T.; Endo, M.; Wakamiya, A.; Kanemitsu, Y. Photocarrier recombination dynamics in perovskite $CH_3NH_3PbI_3$ for solar cell applications. *J. Am. Chem. Soc.* **2014**, *136*, 11610−11613.
(27) Sun, J.; Yang, Y.; Khan, J. I.; Alarousu, E.; Guo, Z.; Zhang, X.; Zhang, Q.; Mohammed, O. F. Ultrafast carrier trapping of a metal-foped titanium dioxide semiconductor revealed by femtosecond transient absorption spectroscopy. *ACS Appl. Mater. Interfaces* **2014**, *6*, 10022−10027.
(28) Righetto, M.; Lim, S. S.; Giovanni, D.; Lim, J. W. M.; Zhang, Q.; Ramesh, S.; Tay, Y. K. E.; Sum, T. C. Hot carriers perspective on the nature of traps in perovskites. *Nat. Commun.* **2020**, *11*, No. 2712.
(29) Carpene, E.; Mancini, E.; Dallera, C.; Schwen, D.; Ronning, C.; De Silvestri, S. Ultrafast carrier dynamics in tetrahedral amorphous carbon: carrier trapping versus electron−hole recombination. *New J. Phys.* **2007**, *9*, 404.
(30) Wang, H.; Zhang, C.; Rana, F. Ultrafast dynamics of defect-assisted electron−hole recombination in monolayer MoS_2. *Nano Lett.* **2015**, *15*, 339−345.
(31) Luo, D.; Su, R.; Zhang, W.; Gong, Q.; Zhu, R. Minimizing non-radiative recombination losses in perovskite solar cells. *Nat. Rev. Mater.* **2020**, *5*, 44−60.
(32) Ball, J. M.; Petrozza, A. Defects in perovskite-halides and their effects in solar cells. *Nat. Energy* **2016**, *1*, No. 16149.
(33) Leijtens, T.; Hoke, E. T.; Grancini, G.; Slotcavage, D. J.; Eperon, G. E.; Ball, J. M.; De Bastiani, M.; Bowring, A. R.; Martino, N.; Wojciechowski, K.; McGehee, M. D.; Snaith, H. J.; Petrozza, A. Mapping electric field-induced switchable poling and structural degradation in hybrid lead halide perovskite thin films. *Adv. Energy Mater.* **2015**, *5*, No. 1500962.
(34) Yoo, J. J.; Seo, G.; Chua, M. R.; Park, T. G.; Lu, Y.; Rotermund, F.; Kim, Y.-K.; Moon, C. S.; Jeon, N. J.; Correa-Baena, J.-P.; Bulovic, V.; Shin, S. S.; Bawendi, M. G.; Seo, J. Efficient perovskite solar cells via improved carrier management. *Nature* **2021**, *590*, 587−593.
(35) Yang, S.; Chen, S.; Mosconi, E.; Fang, Y.; Xiao, X.; Wang, C.; Zhou, Y.; Yu, Z.; Zhao, J.; Gao, Y.; De Angelis, F.; Huang, J. Stabilizing halide perovskite surfaces for solar cell operation with wide-bandgap lead oxysalts. *Science* **2019**, *365*, 473−478.
(36) Zheng, X.; Chen, B.; Dai, J.; Fang, Y.; Bai, Y.; Lin, Y.; Wei, H.; Zeng; Xiao, C.; Huang, J. Defect passivation in hybrid perovskite solar cells using quaternary ammonium halide anions and cations. *Nat. Energy* **2017**, *2*, No. 17102.
(37) Fu, L.; Li, H.; Wang, L.; Yin, R.; Li, B.; Yin, L. Defect passivation strategies in perovskites for an enhanced photovoltaic performance. *Energy Environ. Sci.* **2020**, *13*, 4017−4056.
(38) Dar, M. I.; Arora, N.; Gao, P.; Ahmad, S.; Grätzel, M.; Nazeeruddin, M. K. Investigation regarding the role of chloride in organic−inorganic halide perovskites obtained from chloride containing precursors. *Nano Lett.* **2014**, *14*, 6991−6996.
(39) Williams, S. T.; Zuo, F.; Chueh, C.-C.; Liao, C.-Y.; Liang, P.-W.; Jen, A. K.-Y. Role of chloride in the morphological evolution of organo-lead halide perovskite thin films. *ACS Nano* **2014**, *8*, 10640−10654.
(40) Ni, Z.; Bao, C.; Liu, Y.; Jiang, Q.; Wu, W.-Q.; Chen, S.; Dai, X.; Chen, B.; Hartweg, B.; Yu, Z.; Holman, Z.; Huang, J. Resolving spatial and energetic distributions of trap states in metal halide perovskite solar cells. *Science* **2020**, *367*, 1352−1358.
(41) Haruyama, J.; Sodeyama, K.; Han, L.; Tateyama, Y. Termination Dependence of Tetragonal CH3NH3PbI3 Surfaces for Perovskite Solar Cells. *J. Phys. Chem. Lett.* **2014**, *5*, 2903−2909.
(42) Ran, C.; Xu, J.; Gao, W.; Huang, C.; Dou, S. Defects in metal triiodide perovskite materials towards high-performance solar cells: origin, impact, characterization, and engineering. *Chem. Soc. Rev.* **2018**, *47*, 4581−4610.
(43) Musiienko, A.; Moravec, P.; Grill, R.; Praus, P.; Vasylchenko, I.; Pekarek, J.; Tisdale, J.; Ridzonova, K.; Belas, E.; Landová, L.; Hu, B.; Lukosi, E.; Ahmadi, M. Deep levels, charge transport and mixed conductivity in organometallic halide perovskites. *Energy Environ. Sci.* **2019**, *12*, 1413−1425.
(44) Hoke, E. T.; Slotcavage, D. J.; Dohner, E. R.; Bowring, A. R.; Karunadasa, H. I.; McGehee, M. D. Reversible photo-induced trap formation in mixed-halide hybrid perovskites for photovoltaics. *Chem. Sci.* **2015**, *6*, 613−617.
(45) Hentz, O.; Zhao, Z.; Gradečak, S. Impacts of ion segregation on local optical properties in mixed halide perovskite films. *Nano Lett.* **2016**, *16*, 1485−1490.
(46) Zhao, J. H.; Schlesinger, T. E.; Milnes, A. G. Determination of carrier capture cross sections of traps by deep level transient spectroscopy of semiconductors. *J. Appl. Phys.* **1987**, *62*, 2865−2870.

https://doi.org/10.1021/jacsau.2c00581
JACS Au 2023, 3, 441−448